# Assessment of Geo-positioning Capability of High Resolution Satellite Imagery for Densely Populated High Buildings in Metropolitan Areas

**Gang Qiao, Weian Wang, Bo Wu, Chun Liu, and Rongxing Li**

## Abstract

*This paper analyzes the geo-positioning capability of high-resolution satellite images in a very special metropolitan environment where within a relatively small region there are a large number of densely populated skyscrapers and high buildings. A pair of QuickBird stereo images covering downtown Shanghai were used for analysis. Multi-source data including GPS survey data, aerial images, and lidar data collected in the same area were used for Ground Control Points (GCPs) and Independent Check Points (ICPs) measurements and accuracy analysis. The vendor-provided Rational Function Model followed by a translation and scale correction model in image space was used to introduce the ground control and improve geo-positioning accuracy. The experimental results revealed that there is a clear dependency of geo-positioning accuracy on elevation where the GCPs are placed. Using the vendor-provided RFM and several GCPs across all the elevation ranges improves the overall geo-positioning accuracy.*

## Introduction

The successful launch of satellites with high-resolution imaging capabilities (e.g., Ikonos in 1999, QuickBird in 2001, WorldView-1 in 2007, and GeoEye-1 in 2008) has opened a new era of space imaging for earth observation (Fritz, 1996; Li, 1998; Li *et al.*, 2007). High Resolution Satellite Imagery (HRSI) has been widely used in a variety of applications such as transportation, agriculture, environmental protection, land-use planning, coastal mapping, and disaster monitoring and response (Xu *et al.*, 2003; Di *et al.*, 2003a and 2003b; Warner and Steinmaus, 2005; Al-Khudhalry *et al.*, 2005; Chubey *et al.*, 2006; Mishra *et al.*, 2006; Aguilar *et al.*, 2008a). The use of HRSI in public search systems, such as Google Earth® and Virtual Earth®, has further extended the popularity and applications of HRSI in the daily life of many people. For most applications of HRSI, one of the important parameters considered is its geo-positioning capability, which is also fundamental in photogrammetry and remote sensing applications. Several sensor models, in particular the Rigorous Sensor Model (RSM) and the Rational Function Model (RFM), have been investigated to describe the geometric relationships between imaged objects and the corresponding stereo HRSI scene (Fraser, 1999; Li *et al.*, 2000; Tao and Hu, 2001; Di *et al.*, 2003a; Tao *et al.*, 2004; Wang *et al.*, 2005; Toutin, 2006; Habib *et al.*, 2007; Aguilar *et al.*, 2008b; Li *et al.*, 2009). The RSM explicitly uses both the internal and external orientation parameters of the camera to represent the geometry of the stereo scene formation. However, in many cases it may not be the preferred model to use because of the availability of the orientation parameters, complex expression, and computational considerations (Li *et al.*, 2007; Habib *et al.*, 2007). In many instances (e.g., the Ikonos imagery), an RFM may be the only model provided by an image supplier. The RFM is a mathematical fitting of the RSM using polynomials containing Rational Polynomial Coefficients (RPCs). Usually they are implemented as third-order polynomials consisting of 78 RPCs, which are provided as image metadata by the image supplier. Thus, an RFM can be used as an alternative to the RSM. The quality of HRSI orbital navigation and stability of the data are very high, and resulted in a significantly robust accuracy of the ground points derived from the stereo HRSI images, even without ground control. For example, ground coordinates derived from the RPCs of the Ikonos (GeoLevel) stereo product have shown only a systematic horizontal shift (16 m to 25 m) (Dial, 2000; Di *et al.*, 2003b; Li *et al.*, 2003, 2007, and 2009). The typical QuickBird stereo (Basic Level) imagery also shows a similar shift of 23 m (QuickBird Imagery Products, 2008; Niu *et al.*, 2004). This type of systematic shift can be effectively removed or significantly reduced by use of a few good quality ground control points (GCPs) (Zhou and Li, 2000; Niu *et al.*, 2004; Wang *et al.*, 2005; Aguilar *et al.*, 2007).

Using simulated Ikonos along-track stereo image data, Zhou and Li (2000) demonstrated the potential accuracy of ground points at 3 m ($X$ and $Y$) and 2 m ($Z$) with GCPs, in contrast to an accuracy of 12 m ($X$, $Y$, and $Z$) without GCPs.

Gang Qiao is with the Department of Surveying and Geo-Informatics, Tongji University, P. R. China, and formerly with the Mapping and GIS Laboratory, The Ohio State University (qiaogang@tongji.edu.cn).

Bo Wu is with the Department of Land Surveying & Geo-Informatics, The Hong Kong Polytechnic University, and formerly with Mapping and GIS Laboratory, The Ohio State University.

Weian Wang, and Chun Liu are with the Department of Surveying and Geo-Informatics, Tongji University, P. R. China.

Rongxing Li is with the Mapping and GIS Laboratory, Department of Civil and Environmental Engineering and Geodetic Science, The Ohio State University.

Photogrammetric Engineering & Remote Sensing
Vol. 76, No. 8, August 2010, pp. 923–934.

0099-1112/10/7608–0923/$3.00/0
© 2010 American Society for Photogrammetry and Remote Sensing

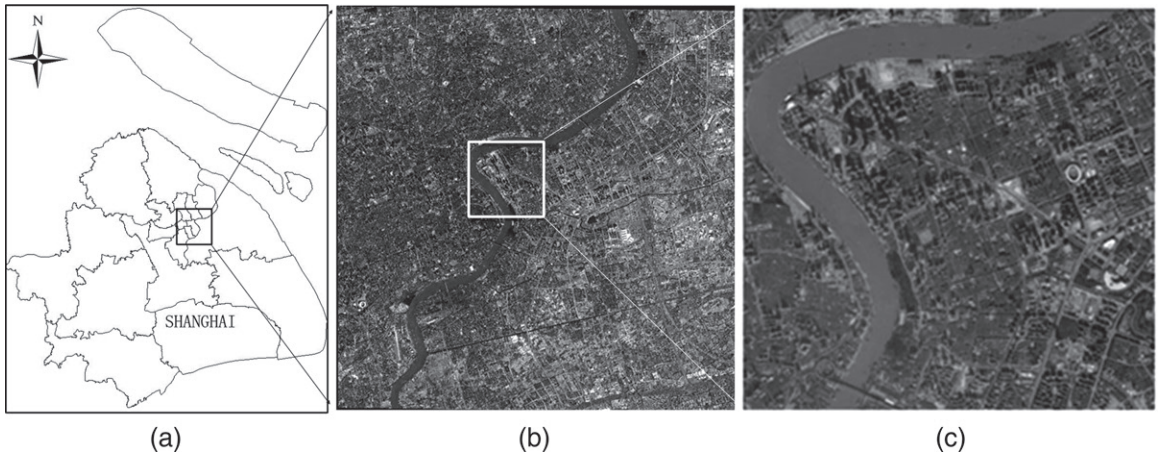


Figure 1. The study area: (a) administrative boundary map of Shanghai, China, (b) downtown Shanghai (QuickBird image), and (c) Lujiazui area, Pudong financial district (enlarged QuickBird image, study area of this paper).

Di *et al.* (2003a) presented the improvement of ground points derived from Ikonos along-track stereo imagery along the southern shore of Lake Erie, Ohio, by employing a few GCPs and achieved a ground accuracy of 1.2 m, 0.9 m, and 1.6 m in *X*, *Y*, and *Z* directions, respectively. Habib *et al.* (2007) investigated the accuracy of ground coordinates over the city of Daejeon, South Korea, using along-track Ikonos stereo imagery; an accuracy of 2 to 3 m was obtained. Qiao *et al.* (2007) presented experimental results of the geo-positioning accuracy using GCPs to improve ground points derived from QuickBird across-track stereo images, and achieved an accuracy of 0.6 m in the *X* and *Y* directions and 0.7 m in the *Z* direction. Similar results have been reported by (Fraser and Hanley, 2005; Hu and Tao, 2002; Toutin, 2004; Jacobsen, 2007)

So far, most of the experiments and results are reported for areas where terrain variations are not dramatic, and GCPs and Independent Check Points (ICPs) are also distributed on the ground without much elevation change. There is lack of investigations and analysis of the HRSI geo-positioning capability in special metropolitan areas where within a small geographic extent there are vast densely populated skyscrapers and high buildings. This paper focuses on issues related to geo-positioning capability analysis of HRSI for areas with a high ratio of elevation range and geographic extent. The study area is downtown Shanghai, China, for which we have collected a stereo pair of cross-track QuickBird images, ground GPS data, high precision aerial mapping images, and lidar data. The integration of these data sets provided a test bed for preparing an answer to the question whether the currently commonly used technique would be appropriate for the special, and important, environment of densely populated high buildings in metropolitan areas. Specific attention has also been paid to obtaining GCPs and ICPs on high buildings from multiple data sets, changes of accuracy in the vertical direction, distribution of GCPs and others. Overall, the results show a clear dependency of geo-positioning accuracy on elevation where the GCPs are placed.

## Study Area and HRSI Dataset

The study area is a relatively small region (latitude 31° 12′ N to 31°15′ N and longitude 121°29′ E to 121° 32′ E) of 11 $km^2$ located in Lujiazui, Pudong district in Shanghai, China (Figure 1). It is a newly built financial district that is about 14 m above sea level and has a relatively flat terrain relief of 1 to 2 m. However, there are a large number of skyscrapers and high buildings (up to 360 m) densely distributed across the region (Figure 2).

In February and May 2004, two strips of QuickBird images (QuickBird Basic Level Product) were collected in the area. They form an across-track stereo image pair. Figure 1b shows the image collected in February 2004. Some selected information about these two images is listed

Figure 2. Densely populated skyscrapers and high buildings in the study area (image source: **www.edushi.com**).

TABLE 1. SELECTED INFORMATION OF THE QUICKBIRD STEREO IMAGE PAIR USED IN THIS STUDY

| Items | Left Image | Right Image |
|---|---|---|
| Acquisition Date | 15 February 2004 | 05 May 2004 |
| Acquisition Time | 02:30:28 | 02:26:18 |
| Scan Direction | Forward | Forward |
| Product Level | Basic | Basic |
| Image Size (pixels*pixels) | 27552 * 25776 | 27552 * 25952 |
| Along-Track View Angle (°) | 19.8 | 14.6 |
| Cross-Track View Angle (°) | -5.5 | 19.6 |
| Off Nadir View Angle (°) | 20.6 | 24.4 |
| Pixel Resolution (m) | 0.682 | 0.717 |
| Satellite Azimuth Angle (°) | 353.9 | 60.4 |
| Satellite Elevation Angle (°) | 68.2 | 64.0 |
| Convergence Angle (°) | 25.9 | |

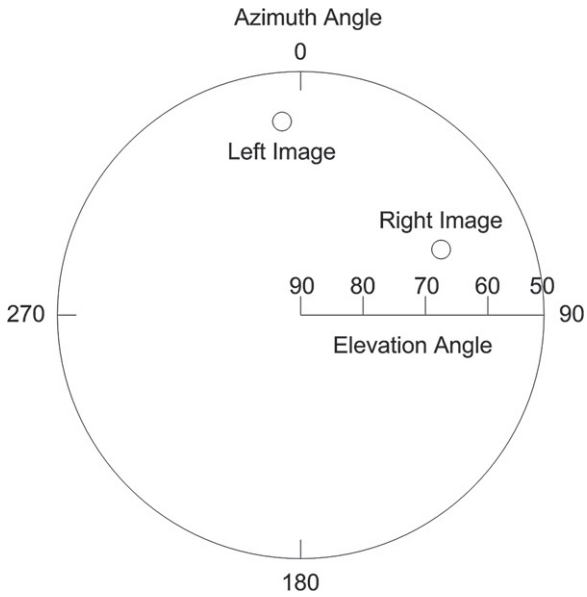


Figure 3. Relative positions and pointing angles of the two orbits with respect to the study area center.

in Table 1. The relative positions and pointing angles of the two orbits with respect to the study area center are illustrated in Figure 3. Most of the information, such as azimuth and elevation angles, is provided in the metadata files. Using the azimuth and elevation angles and a set of equations in Li *et al.* (2007), the convergence angle between the two images is calculated as 25.9°, indicating that they are suitable to form a good quality stereo pair for geo-positioning capability analysis.

## GCP and ICP Measurements from Multi-source Data

We have collected multi-source data in the study area, including ground GPS survey data, aerial mapping images, and lidar data. Figure 4 illustrates the coverage of these data sets. In our analysis, GPS-surveyed points were used as GCPs and ICPs on the ground while points located on the buildings as measured from the aerial images and lidar data were used as GCPs and ICPs at higher elevations.

### Ground GPS points

A GPS survey campaign was conducted in the downtown Shanghai area on 30 December 2006, supported by the Virtual Reference Station (VRS) technology (Wanninger, 2003) provided by the Shanghai Surveying and Mapping Institute. In total, 82 points were surveyed which are evenly distributed in the area. These surveyed points are distinguishing features, such as street corners that can be identified both on images and on the ground. Among them, 22 points were used in the following aerial image processing, and 13 were used to process the QuickBird images in the study area. The overall accuracy of these GPS points is 0.05 to 0.1 m in all three directions. The distribution of the ground GPS points is shown in Figure 5.

### Integration of Aerial Images and Lidar Data for Measurement of Points on High Buildings

Points with known coordinates on the high buildings in the study area are needed for the study and analysis. Access to the buildings and feasibility of placement of instruments on these points could not be warranted for all points designed. The alternative was to use noncontact measurements from the multiple data sources such as aerial images and lidar data. First, a photogrammetric bundle adjustment of the aerial images was performed and the footprints of the buildings were extracted from the bundle adjusted aerial images. Second, after a registration of the buildings in both aerial images and the lidar data, the vertical coordinates of the points on the buildings were obtained from the lidar data. Since the aerial images possess sharp buildings edges and have a generally higher horizontal accuracy, the horizontal coordinates of the building points were taken from building boundary measurements of the bundle adjusted aerial images. Finally, the corresponding vertical coordinates of the points were obtained from lidar data, considering the very high accuracy of lidar measurements.

A total of 26 aerial images with a ground resolution of 0.22 m were employed to form an aerial image network for bundle adjustment. These images were taken using an Intergraph Digital Mapping Camera (DMC) by the Shanghai Surveying and Mapping Institute on 28 September 2006. The bundle adjustment was performed using the ERDAS Leica Photogrammetry Suite. A total of 22 ground GPS points on the ground were utilized in the adjustment, 6 as GCPs and 16 as ICPs (Figure 6). After the bundle adjustment, the computed ground coordinates of the ICPs were compared with the corresponding ground GPS points. The RMSEs (root mean square errors) computed from the ICPs are 0.18 m in the $X$ direction, 0.20 m in the $Y$ direction, and 0.39 m in the $Z$ direction. This accuracy is sufficient for integration with the lidar data and further use in QuickBird geo-positioning accuracy analysis.

The lidar point cloud data in an area of 20 km$^2$ (Figure 4) were acquired in February, 2006, by Shanghai Surveying and Mapping Institute using an ALTM3100 lidar system from Optech, Inc. The lidar survey was comprised of nine east-west strips and six north-south strips with a 900 m flying height. The scan angle is 20° and the resolution is about 50 points/m$^2$. The accuracy of the lidar data is 0.15 m to 1.00 m in the $X$ and $Y$ directions, and 0.10 m in the $Z$ direction. The vertical accuracy of the lidar points is better than that obtained from the aerial images (0.39 m). Therefore, we combined the vertical information from the lidar data with the horizontal information from the aerial images for these points on the building rooftops. Both the aerial images and lidar data were referenced to the WGS84 frame. The correspondence is implemented as an interactive measurement and matching process. First, an aerial stereo pair can be displayed and the building to be measured can be zoomed into

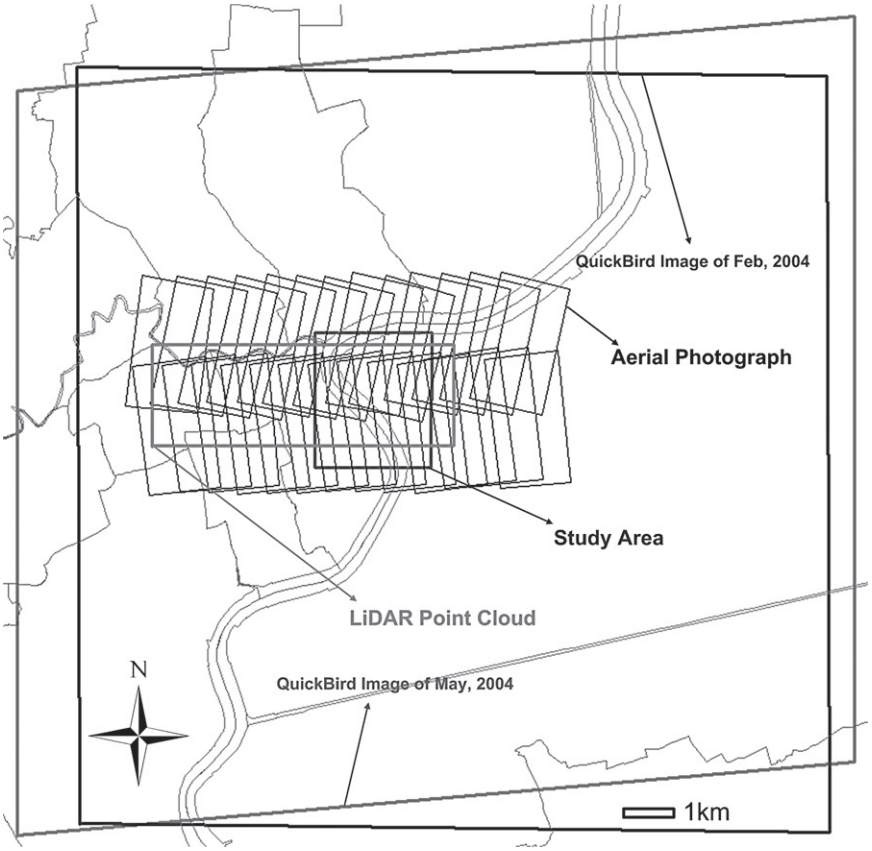


Figure 4. Coverage of the involved multi-source data (QuickBird images, aerial photographs, lidar point cloud, and the study area).

(Figure 7). A rooftop point, for example, can be measured to compute its 3D coordinates. Then the lidar data can be plotted in 3D with a viewing position and angles that are close to those of the aerial images. Identification of the same rooftop point in the lidar data was done manually by observing the building in 3D view with different looking angles. Only the buildings with flat rooftop or roof edges were selected in our research. The elevation of the rooftop points were determined as follows: first, within a small window around the rooftop point, a number of lidar points (usually more than 20 in our research) with their elevation value differences less than 0.05 m, were selected as on the same rooftop. Then, the elevation of the rooftop point was determined to be the average elevation value of these points. The elevation of the rooftop point from the lidar data is then combined with its horizontal coordinates of the same point from photogrammetric triangulation using the aerial images. Using this approach of manual registration between stereo aerial images and lidar data, GCPs and ICPs on rooftops can be obtained for both planar and vertical accuracy analysis.

A total of 88 points (including GPS points) were measured and identified in the study area, which will serve as GCPS and ICPs for a further HRSI experiment. Thirteen of these points are located on the ground (elevation about 14 m). The rest of the points are building rooftop points that have elevations of 20 m to 360 m. The elevations of the points are listed in Table 2. Figure 8 illustrates the building heights and locations of the points.

## Experiments with HRSI Images and Analysis

Figure 9 shows the overall strategy of this study. The aerial images and lidar data are preprocessed and integrated as described in the previous sections to produce GCPs used in the following HRSI data analysis. The QuickBird stereo images came with RPCs (Rational Polynomial Coefficients) and can be used to provide a solution for calculating 3D coordinates of ground points measured from the HRSI images without GCPs. An improvement of the accuracy of the ground points thus obtained can be conducted by using a correction model in the image space and a small number of GCPs. In particular, a translation and scale correction model is applied. To analyze the effectiveness of the correction model with respect to various elevations, the GCPs derived from the GPS survey data, aerial images, and lidar data are further categorized into groups of GCPs and ICPs at different elevations. Finally, the correction model can be tested and analyzed using the HRSI measurements and the ground GCPs and ICPs for various scenarios. In detail, four experiments were conducted for this study. First, we analyzed the HRSI geo-positioning capability without involvement of any GCP. Second, we analyzed the HRSI geo-positioning capability with GCPs only on the ground. Third, the HRSI geo-positioning capability with GCPs located on building rooftops at individual heights was investigated. Finally, the HRSI geo-positioning capability with GCPS at all heights together was examined.

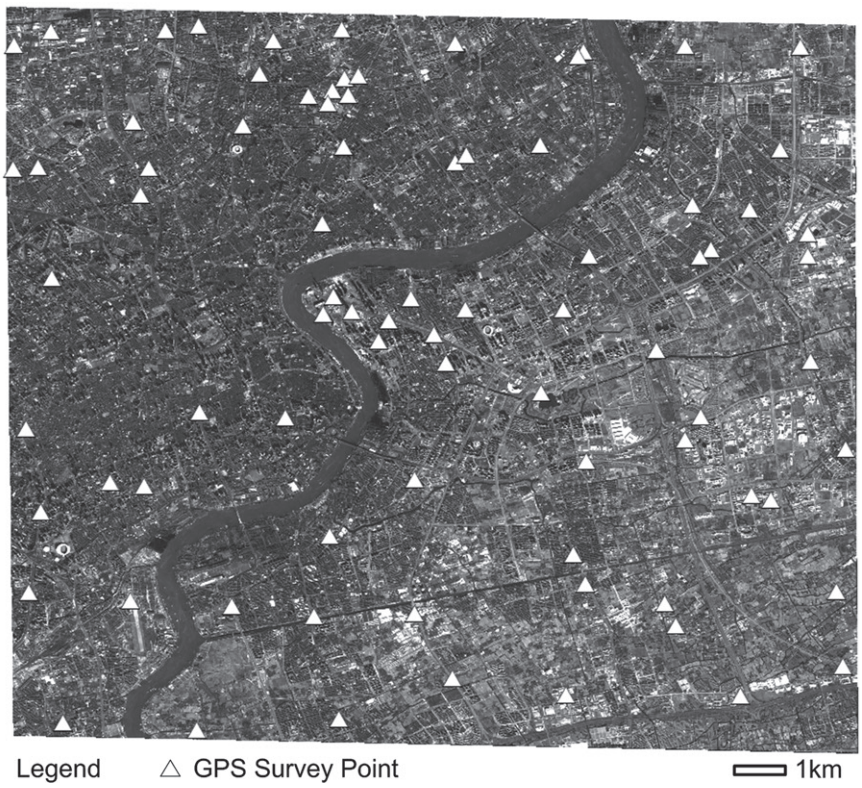


Figure 5. Distribution of the ground GPS points.


Figure 6. Coverage of the 26 aerial images and distribution of GCPs and ICPs for photogrammetric bundle adjustment.

**Geo-positioning Accuracy without GCPs**

For the above-mentioned 88 GCPs and ICPs with known ground coordinates computed from GPS survey data, aerial photogrammetric bundle adjustment, and lidar data, the corresponding image coordinates in the QuickBird stereo pair were measured. Using the RPCs contained in image metadata and the measured image coordinates, 3D ground coordinates of the 88 points were calculated. They were compared with the known coordinates. The differences between the known ground coordinates and the RFM-derived coordinates were employed to compute the RMSE:

$$RMSE = \sqrt{\frac{\sum_{i=1}^{n} v_i^2}{n-1}} \tag{1}$$

where $n$ is the number of points used in the calculation, and $v_i$ is the coordinate difference. The result for all of the 88 points mentioned above is listed in Table 3.

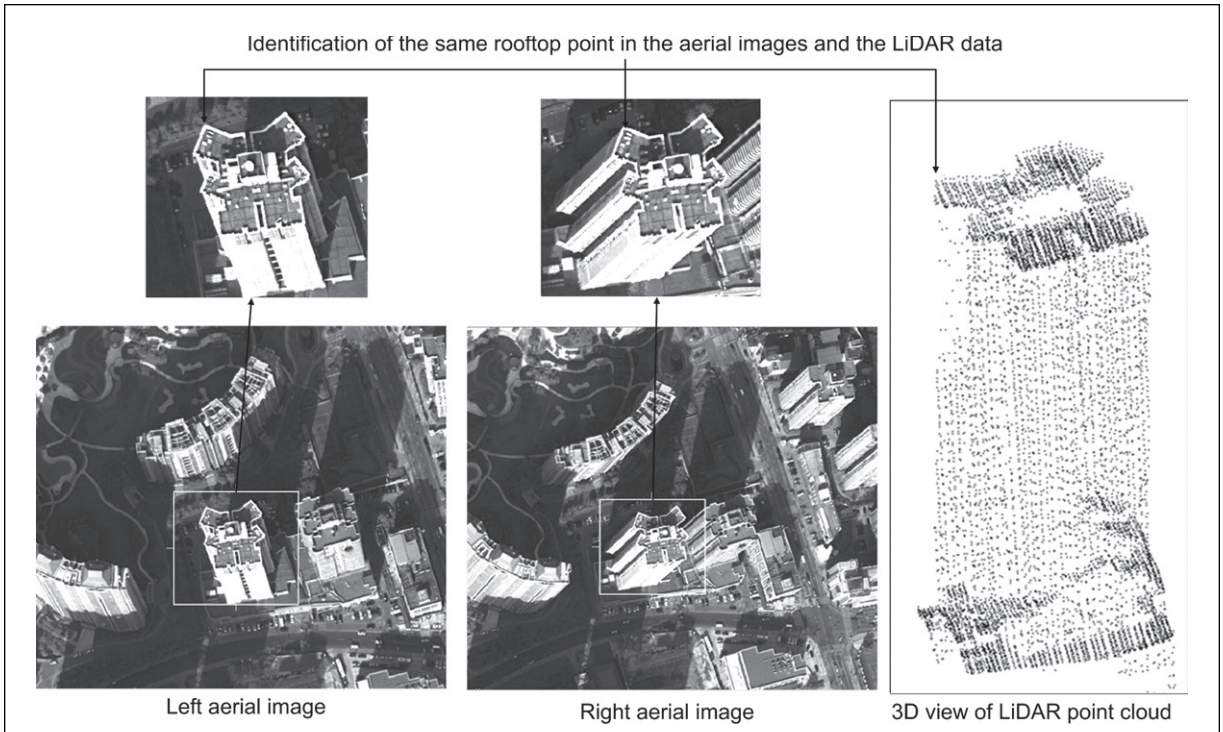


Figure 7. A stereo aerial image pair, zoomed area of a high building, and 3D display of the building using lidar data for multi-source data supported rooftop point identification and measurement.

TABLE 2. ELEVATIONS OF THE MEASURED GCPS AND ICPS

| ID | Elevation (m) | ID | Elevation (m) | ID | Elevation (m) | ID | Elevation (m) |
|---|---|---|---|---|---|---|---|
| 1 | 12.92 | 23 | 76.65 | 45 | 102.48 | 67 | 130.66 |
| 2 | 13.15 | 24 | 77.07 | 46 | 103.77 | 68 | 135.63 |
| 3 | 13.25 | 25 | 77.79 | 47 | 104.47 | 69 | 137.05 |
| 4 | 13.35 | 26 | 78.20 | 48 | 107.36 | 70 | 137.16 |
| 5 | 13.38 | 27 | 79.80 | 49 | 109.63 | 71 | 139.12 |
| 6 | 13.55 | 28 | 84.42 | 50 | 109.97 | 72 | 151.15 |
| 7 | 13.56 | 29 | 85.06 | 51 | 110.03 | 73 | 153.53 |
| 8 | 13.62 | 30 | 85.51 | 52 | 111.04 | 74 | 154.18 |
| 9 | 13.77 | 31 | 85.97 | 53 | 112.04 | 75 | 154.46 |
| 10 | 13.80 | 32 | 86.43 | 54 | 112.30 | 76 | 162.63 |
| 11 | 14.23 | 33 | 86.51 | 55 | 113.66 | 77 | 163.81 |
| 12 | 14.48 | 34 | 87.04 | 56 | 115.01 | 78 | 164.17 |
| 13 | 15.38 | 35 | 88.21 | 57 | 115.14 | 79 | 181.31 |
| 14 | 51.44 | 36 | 88.24 | 58 | 116.25 | 80 | 189.25 |
| 15 | 54.80 | 37 | 88.25 | 59 | 118.59 | 81 | 190.81 |
| 16 | 64.69 | 38 | 88.28 | 60 | 119.65 | 82 | 192.20 |
| 17 | 69.91 | 39 | 88.59 | 61 | 121.92 | 83 | 193.82 |
| 18 | 70.00 | 40 | 88.62 | 62 | 121.94 | 84 | 201.38 |
| 19 | 73.81 | 41 | 89.79 | 63 | 122.52 | 85 | 212.67 |
| 20 | 74.55 | 42 | 89.97 | 64 | 125.64 | 86 | 214.11 |
| 21 | 75.04 | 43 | 96.23 | 65 | 127.05 | 87 | 244.64 |
| 22 | 75.49 | 44 | 102.39 | 66 | 130.04 | 88 | 360.76 |

From Table 3, it can be seen that the RMSE in the latitude direction is about 14 m and longitude about 21 m. The combined horizontal RMSE is about 24 m. This magnitude and the range are consistent with the specification published by DigitalGlobe, Inc. for the stereo image product (QuickBird Imagery Products, 2008) and in line with similar results reported by other researchers as mentioned previously. The RMSE in the vertical direction is 17 m which is of the same order as that in horizontal directions.

### Geo-positioning Accuracy with GCPs on the Ground

Using GCPs, the ground coordinates of the points determined by the RFM above can be improved. This is usually implemented by a correction model either in the object space to correct the triangulated ground coordinates or in the image space to correct the image coordinates of the points. In this study we adopt the correction model in the image space as described in (Wang *et al.*, 2005; Li *et al.*, 2007).

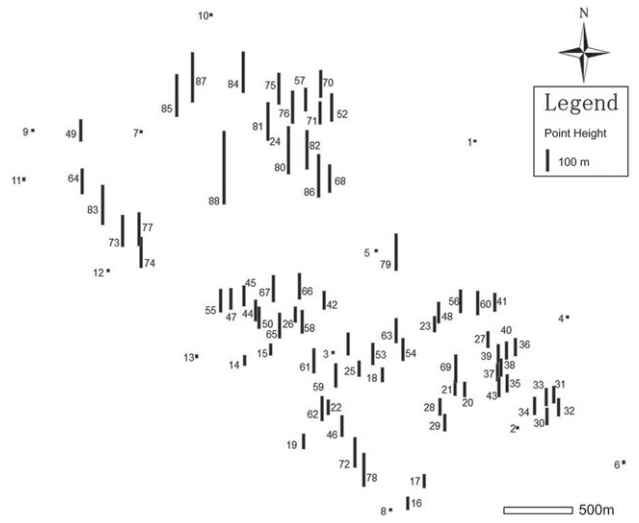


Figure 8. Building heights and locations of the rooftop points measured from GPS, aerial stereo images, and lidar data in the study area (numbers are point IDs).

The geometric correction in the image space was implemented by adding additional parameters into the RFM model to adjust for inconsistencies caused by imperfect pointing data from the orbits. In Equation 2, a translation correction and a scale correction are added to each image coordinate of $r$ (row) and $c$ (column) of a point in the rational function-based photogrammetric collinearity equations:

$$r + a_0 + a_1 r = \frac{P_1(X,Y,Z)}{P_2(X,Y,Z)}$$
$$c + b_0 + b_1 c = \frac{P_3(X,Y,Z)}{P_4(X,Y,Z)} \quad (2)$$

TABLE 3. RMSE OF GROUND COORDINATES WITHOUT USING GCPS

| Accuracy | Latitude (m) | Longitude (m) | Horizontal (m) | Vertical (m) |
|---|---|---|---|---|
| Min | 12.75 | 18.99 | 22.33 | 14.39 |
| Max | 14.83 | 24.37 | 25.84 | 18.73 |
| RMSE | 13.91 | 20.69 | 23.75 | 17.00 |

where $X,Y,Z$ are the latitude, longitude, and ellipsoidal height of the point in the WGS84 frame, and $P_i(i = 1,2,3,4)$ is a third-order, 20-term polynomial containing 78 RPCs provided in the image metadata. Variables $a_0$, $a_1$, $b_0$, and $b_1$ are the parameters for the translation and scale correction model.

Four GCPs on the ground with an average elevation of about 13 m were selected and are shown as triangles in Figure 10a. Other points were employed as ICPs and are illustrated as black bars. First, a GCP with known ($X$, $Y$, $Z$) was incorporated into the right-hand side of Equation 2 and evaluated, and its corresponding image coordinates ($r$, $c$) were put into the left-hand side, while $a_0$, $a_1$, $b_0$, and $b_1$ were treated as unknowns. For the four GCPs, we can establish eight equations to solve for four unknowns by a least-squares solution. Then, the estimated translation and scale parameters along with the RFM polynomials (Equation 2) can be used for the computation of geometrically corrected ground coordinates for any points when their image coordinates are measured. Finally, the geo-positioning accuracy of this approach was assessed by using the ICPs. The images coordinates of the ICPs were all measured. Employing Equation 2 with the translation and scale parameters, we computed the ground coordinates of the ICPs, which were then compared with the known ground coordinates. The horizontal accuracy has not shown much variation in this study. We focus on the vertical accuracy analysis with significant height variations in a small geographic extent.

Figure 10 shows the analysis result of the above correction model in this study area. The black bars in Figure 10a describe the elevations of the ICPs (buildings) along with their point IDs. The elevation differences were calculated

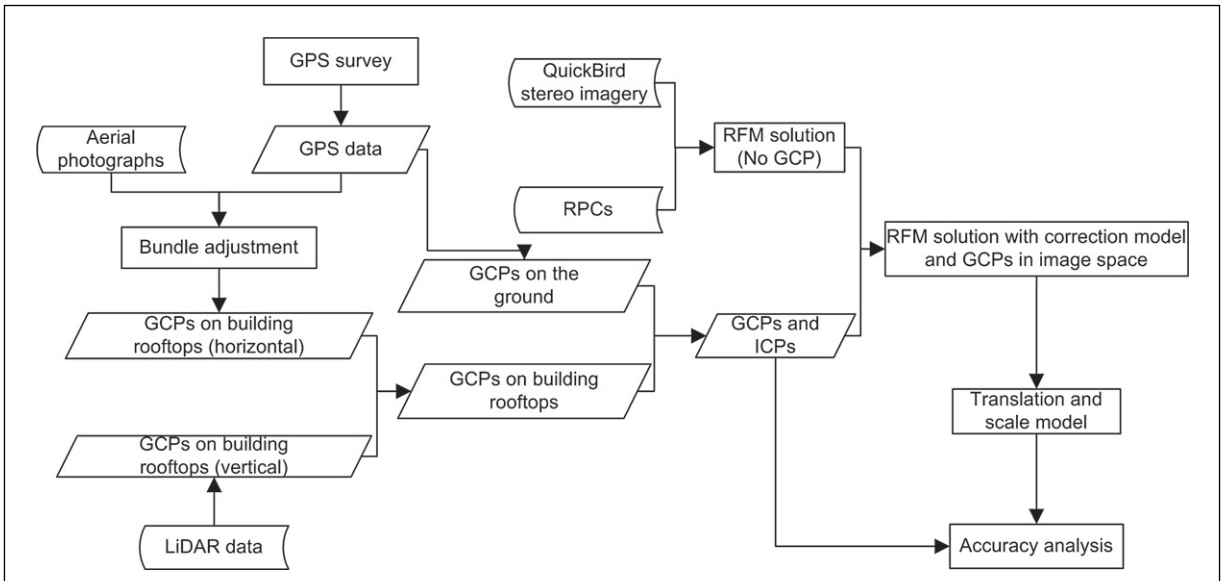


Figure 9. Concept of the study strategy for HRSI geo-positioning capability analysis.

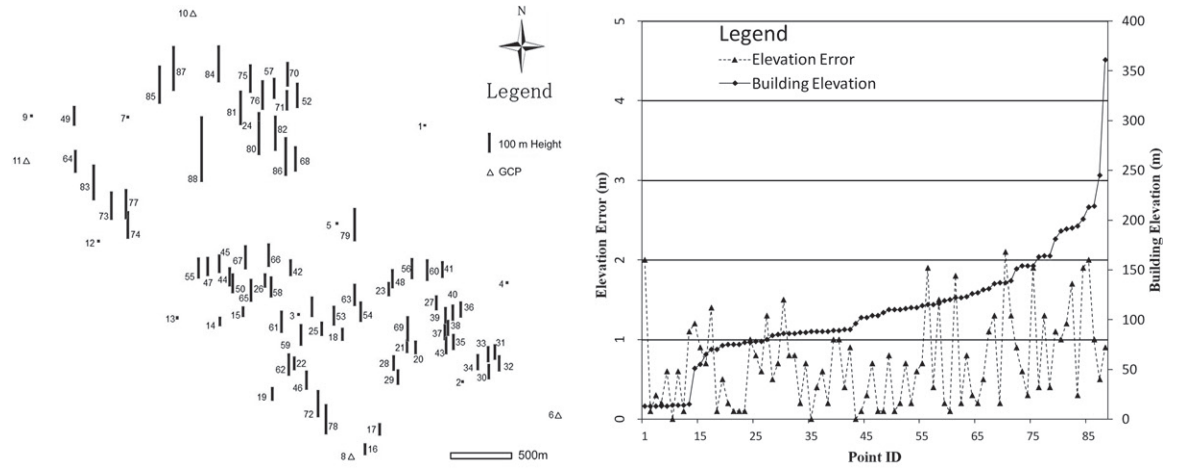


Figure 10. HRSI geo-positioning accuracy with GCPs on the ground: (a) point distribution with point IDs, 4 GCPs (triangles) and 84 ICPs (black bars), and (b) relationship between the elevation error and the building height.

from the known coordinates and the improved RFM with the translation and scale parameters. The RMSE of the differences is 0.9 m with a maximum of 2.1 m. This result is an improvement over the RMSE of 17 m in Table 3 for the case of geo-positioning without any GCPs. However, it is not as good as the accuracy (RMSE = 0.6 m), for example, reported in (Li *et al.*, 2007) for another QuickBird stereo pair. Figure 10b shows the relationship between the elevation differences and the corresponding building heights. Note that the ICPs are numbered in an ascending order according to the elevation. There is a general trend of the elevation error (RMSE) to increase with respect to the building height (elevation) increase. This is further verified by observing the relationship using smaller elevation intervals. We divided all the ICPs into five different elevation ranges: 0 to 50 m, 50 to 100 m, 100 to 150 m, 150 to 200 m, and 200 to 361 m (Table 4). Within each elevation range, we calculate an average difference between the known coordinates and those improved by the translation and scale correction model (Figure 11).

From Figure 11 we can clearly see that the average elevation error increases as the elevation of the five building groups increases. Since the GCPs are on the ground (average elevation 13.8 m), the first group which has ICPs on the ground (average elevation 13.7 m) has a minimum elevation error of 0.57 m. On the other side, the average elevation error reaches a maximum of 1.28 m for the fifth group of buildings (average elevation 246.7 m).

It should be noted that we also compared results from the RFM followed by improvement using several correction models including a translation model, scale and translation model, and affine transformation model using the same dataset. The experimental results revealed that there is no significant difference among these models, as also reported by Di *et al.* (2003a) and Wang *et al.* (2005). Therefore, we only present the results from using the translation and scale model in this paper.

TABLE 4. FIVE GROUPS OF POINTS (GCPS AND ICPS) USED FOR GEO-POSITIONING ACCURACY AND ELEVATION DEPENDENCY ANALYSIS

| Elevation Range (m) | 0–50 | 50–100 | 100–150 | 150–200 | 200–361 |
|---|---|---|---|---|---|
| Number of points | 13 | 30 | 28 | 12 | 5 |
| Min Elevation (m) | 12.92 | 51.44 | 102.39 | 151.15 | 201.38 |
| Max Elevation (m) | 15.38 | 96.23 | 139.12 | 193.82 | 360.76 |
| Average Elevation (m) | 13.73 | 80.21 | 118.30 | 170.94 | 246.71 |

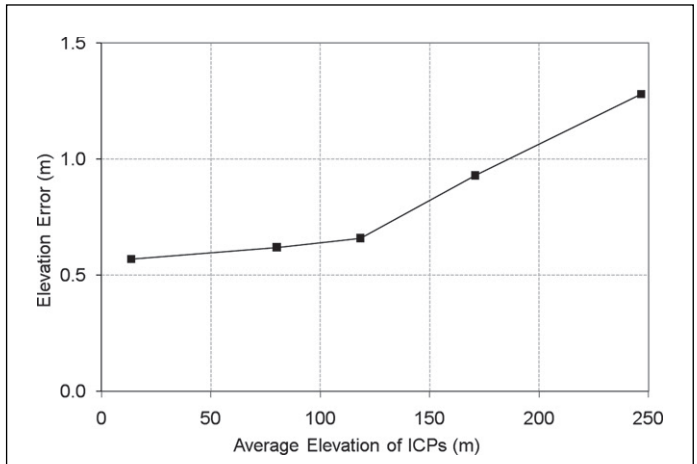


Figure 11. Increase of elevation error with respect to five groups of buildings at different elevations in the case of the translation and scale correction model with GCPs on the ground.

**Geo-positioning Accuracy with GCPs at Different Elevations of Building Groups**

This section describes how GCPs located at different elevations of the building groups in Table 4 can affect the geo-positioning accuracy.

For each elevation range in Table 4, four evenly distributed points within the range were selected as GCPs. The RFM model followed by a translation and scale model in the image space were employed by using the four GCPs for geometric improvement. All other points in the same range and other

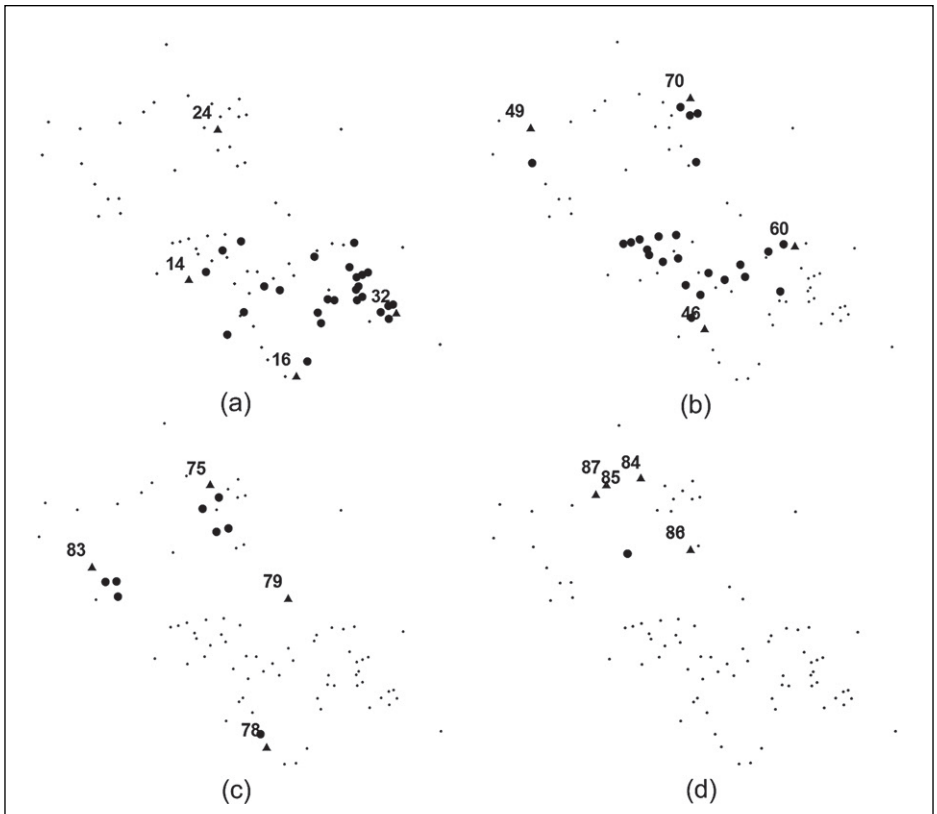


Figure 12. Distribution of the GCPs and ICPs in four cases of geo-positioning accuracy and elevation dependence analysis using four groups of GCPs with elevations: (a) 50 to 100 m, (b) 100 to 150 m, (c) 150 to 200 m, and (d) 200 to 361 m.

four ranges were utilized as ICPs to analyze the effectiveness of the GCPs at one elevation group on ICPs at the same and different elevation groups. Since the results from the GCPs on the ground elevation were described in the previous section, this section only gives the results from GCPs located on the building rooftops. Figure 12 shows the distribution of the GCPs and ICPs of the four cases with GCPs at four elevation ranges. The triangles and point IDs in each sub-figure denote the GCPs used in the same elevation range. The larger dots are the remaining points within the same elevation range, which were used as ICPs. The smaller dots illustrate the points in other elevation ranges that were also utilized as ICPs.

As shown in Table 5, four GCPs (point IDs in Figure 12a) with an average elevation of 69.91 m were used to improve the ground coordinate accuracy by the RFM and the translation and scale model. The resulting translation and scale coefficients were employed to compute the ground coordinates of the ICPs that were separated into five elevation groups at average elevations of 13.72 m, 81.80 m, 118.31 m, 170.95 m, and 246.71 m. These estimated coordinates were compared with the known coordinates within each group. Their differences were used to calculate the average elevation errors in the five ICP groups (first row in Table 5). The same process is employed to produce data in the following three rows in Table 5.

As can be seen in Table 5, there is a clear relationship between the average elevation errors and elevations of the GCPs. For example, for the first case (elevation range 50 to 100 m), the average elevation of the GCPs is 69.91 m. The minimum error of 0.59 m appears when using the ICPs within the same range of that of the GCPs (50 to 100 m), while the elevation error increases as the elevations of the ICPs are farther away from those of the GCPs. The maximum of 0.88 m appears in the ICP elevation range of 200 to 361 m, which is farthest from the GCPs (50 to 100 m). This same trend continues as we observe the other three cases

TABLE 5. AVERAGE ELEVATION ERRORS OF THE FOUR CASES OF GEO-POSITIONING ACCURACY AND ELEVATION DEPENDENCE ANALYSIS USING FOUR GROUPS OF GCPS

| GCP Elev Range & (Avg. Elevation) | Average Elevation Error Estimated by Using ICPs in Elevation Group | | | | |
|---|---|---|---|---|---|
| | 0–50 m | 50–100 m | 100–150 m | 150–200 m | 200–361 m |
| 50–100 m (69.91 m) | 0.69 | 0.59 | 0.68 | 0.85 | 0.88 |
| 100–150 m (117.55 m) | 0.94 | 0.69 | 0.61 | 1.01 | 0.97 |
| 150–200 m (173.44 m) | 0.78 | 0.81 | 0.75 | 0.67 | 1.00 |
| 200–361 m (218.20 m) | 1.06 | 0.97 | 0.95 | 0.87 | 0.41 |

of GCP elevation ranges in Table 5. Therefore, the RFM with a translation and scale correction model performs differently when the GCPs are placed at different elevations. The determined ground points have the highest accuracy when they are within the elevation range of the GCPs.

**Geo-positioning Accuracy with GCPs Across Different Elevation Ranges**

To examine the overall influence of the GCPs across different elevation ranges on the geo-positioning accuracy, we randomly selected 25 sets of four points as GCPs and the rest 84 points as ICPs from the dataset in Table 2. The variation of the calculated elevation errors of the ICPs with respect to the elevation range of the used GCPs is shown in Figure 13.

Figure 13 shows a general trend that the elevation error of the ICPs is related to the elevation range of the GCPs. The elevation error of the ICPs is smaller when the average elevation of the GCPs is close to the middle of the whole elevation range (100 to 150 m) in the study area, and is greater when the average elevation of the GCPs reaches the two boundaries (0 to 50 m and 250 to 300 m). This means that the GCPs should be "representative" of the object model.

The above-mentioned dependency of geo-positioning accuracy on the elevations of the GCPs used provoked an experiment of geo-positioning by the RFM and the translation and scale model using GCPs across precisely all the five elevation ranges from the ground to the high building rooftops in this study area.

Five evenly distributed GCPs, one from each of the five elevation ranges, were selected to serve as GCPs. These GCPs (point IDs 8, 32, 49, 79, and 84) are shown in Figure 14, with their elevations indicated by the heights of the bars. All the other measured points were used as ICPs. The experimental result is shown in Table 6.

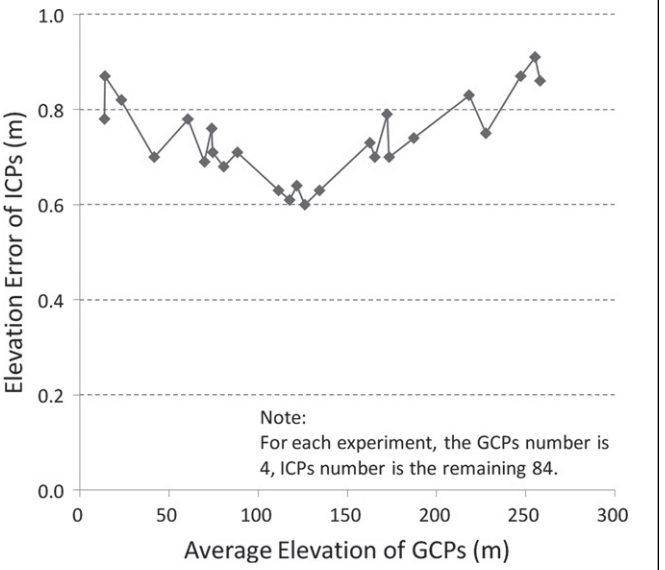


Figure 13. Relationship between the elevation ranges of the GCPs and the elevation errors of the ICPs.

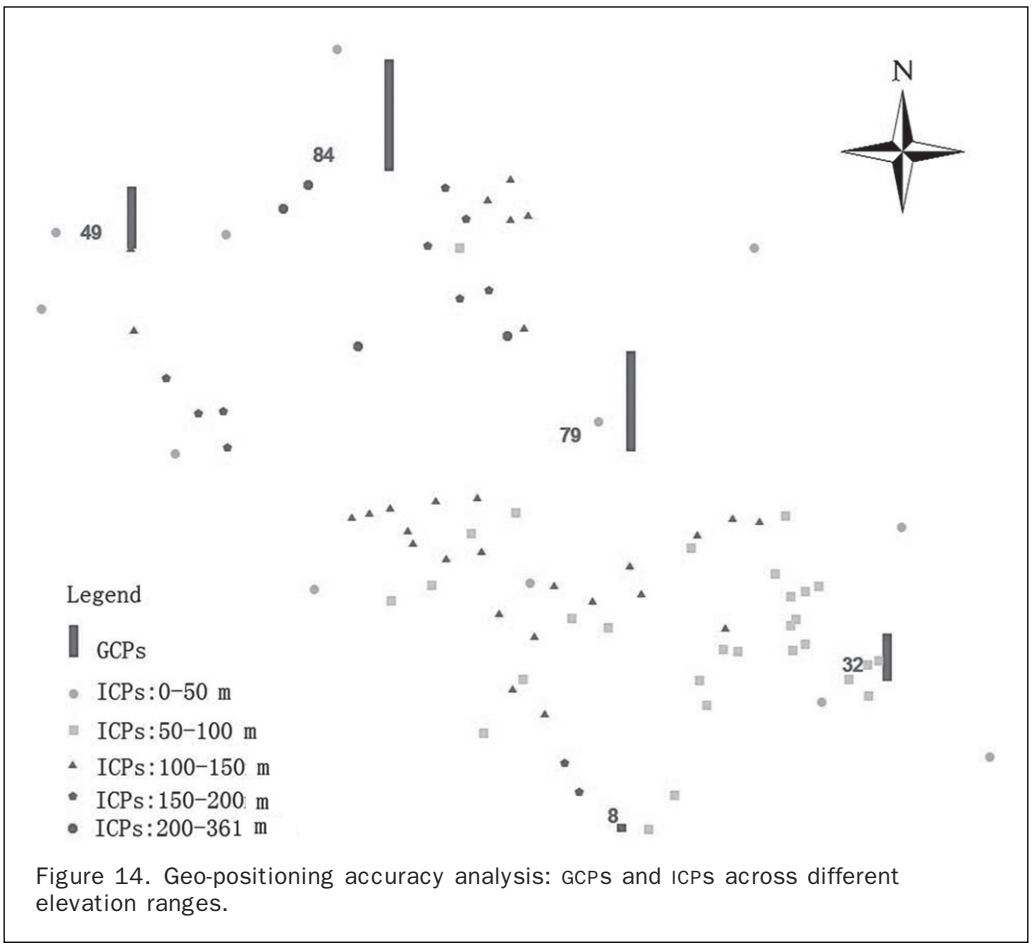


Figure 14. Geo-positioning accuracy analysis: GCPs and ICPs across different elevation ranges.

TABLE 6. RESULTS OF GEO-POSITIONING EXPERIMENT WITH GCPS AND ICPS ACROSS DIFFERENT ELEVATION RANGES

| | Average Elevation Error Estimated by Using ICPs in Elevation Group | | | | |
|---|---|---|---|---|---|
| GCP ID & (Average Height) | 0–50 m | 50–100 m | 100–150 m | 150–200 m | 200–361 m |
| 8 32 49 79 84 (126.65 m) | 0.88 | 0.93 | 0.81 | 0.72 | 1.00 |

As shown in Table 6, the elevation error in this experiment ranges from 0.72 m to 1.00 m and is of about the same order as those in Table 5. However, they are higher than the elevation errors at the minimum levels where the GCPs were selected (0.59 m, 0.61 m, 0.67 m, 0.41 m) in Table 5. The use of GCPs across different elevation ranges did not improve the geo-positioning accuracy, but resulted in a relatively even distribution of the residuals to all ICPs across the elevation ranges.

## Conclusions and Future Research

This paper presents the results of geo-positioning capability analysis for HRSI in a very special metropolitan environment in Shanghai, China, where within a relatively small region there are a large number of very densely populated skyscrapers and high buildings. Using QuickBird stereo imagery along with GPS survey data, aerial images, and lidar data covering the same test area, the experimental results allow us to draw the following conclusions.

1. Using a cross-track QuickBird stereo image pair and the vendor-provided RFM model, a ground geo-positioning accuracy of 23 to 24 m in horizontal and 17 m in vertical directions is achieved without any GCPs. This estimated accuracy is in line with the vendor's technical specification and early publications (QuickBird Imagery Products, 2008; Niu *et al.*, 2004; Li *et al.*, 2007; Fraser and Hanley, 2005).
2. Using a few GCPs along with the vendor-provided RFM and the translation and scale correction model, the geo-positioning accuracy in the vertical direction can be improved to a sub-meter level for ground points up to 200 m in elevation and an accuracy of 1.3 m for points between 200 m and 361 m. This model and the few GCPs are capable of correcting the majority of the pointing errors and inconsistencies resulting from the orbital data. Since the GCPs used are all on the ground, the best accuracy is achieved for points also on or close to the ground, while the elevation error increases as the elevation of the points increases.
3. It is further found that the performance of the above correction model depends on the vertical distribution of the GCPs employed, which are selected sequentially at five different elevation levels of the buildings for this study. The RMSE achieves a minimum at the elevation close to where the GCPs are located. Consequently, the RMSE reaches the maximum for the points that are farthest from the GCPs.
4. Using the vendor-provided RFM and the GCPs across all the elevation ranges improves the overall geo-positioning accuracy. However, the overall RMSE is not better than that of the individual experiments where the GCPs are placed at a particular elevation level.

Overall, the method of improvement of geo-positioning accuracy by using the vendor-provided RFM and a simple correction model with few GCPs performs well to some degree in a special metropolitan region where skyscrapers and high buildings are densely populated. The results show a clear dependency of geo-positioning accuracy on elevation where the GCPs are placed. This dependency does not disappear even with GCPs distributed across the entire elevation range of the region.

## Acknowledgments

The research was supported by the National 863 Project "Complicated Features' Extraction and Analysis from Central Districts in Metropolis" of China (No: 2007AA12Z178), Tongji University "985" Project Sub-system "Integration Monitoring for City Spatial Information", the Scientific Research Foundation of Key Laboratory for Land Environment and Disaster Monitoring of SBSM (Grant No. LEDM2009B02), the Key Lab of Spatial Data Mining & Information Sharing of Ministry of Education (Grant No. 201004), and funding project No. 200713 of the Key Laboratory of Geo-Informatics of State Bureau of Surveying and Mapping, China. The authors appreciate Shanghai Surveying and Mapping Institute for providing the aerial images and LiDAR point cloud data. We also would like to thank Mr. Xiling Li from the Shanghai Euroasia Group for his work on GPS surveying and related data processing.

## References

Aguilar, M.A., F.J. Aguilar, F. Agüera, and J.A. Sánchez, 2007. Geometric accuracy assessment of Quick-Bird basic imagery using different operational approaches, *Photogrammetric Engineering & Remote Sensing*, 73(12):1321–1332.

Aguilar, M.A., F. Agüera, F.J. Aguilar, and F. Carvajal, 2008a. Geometric accuracy assessment of the orthorectification process from very high resolution satellite imagery for common agricultural policy purposes, *International Journal of Remote Sensing,* 29(24):7181–7197.

Aguilar, M.A., F.J. Aguilar, and F. Agüera, 2008b. Assessing geometric reliability of corrected images from very high resolution satellites, *Photogrammetric Engineering & Remote Sensing*, 74(12):1551–1560.

Al-Khudhalry, D.H.A., I. Caravaggi, and S. Glada, 2005. Structural damage assessments from Ikonos data using change detection, object-oriented segmentation, and classification techniques, *Photogrammetric Engineering & Remote Sensing*, 71(7):825–837.

Chubey, M.S., S.E. Franklin, and M.A. Wulder, 2006. Object-based analysis of Ikonos-2 imagery for extraction of forest inventory parameters, *Photogrammetric Engineering & Remote Sensing*, 72(4):393–394.

Dial, G., 2000. IKONOS satellite mapping accuracy, *Proceedings of the 2000 Annual ASPRS Convention*, 22–26 May, Washington, D.C., unpaginated CD-ROM.

Di, K., R. Ma, and R. Li, 2003a. Rational functions and potential for rigorous sensor model recovery, *Photogrammetric Engineering & Remote Sensing*, 69(1):33–41.

Di, K., R. Ma, and R. Li, 2003b. Geometric processing of Ikonos stereo imagery for coastal mapping applications, *Photogrammetric Engineering & Remote Sensing*, 69(8):873–879.

Fraser, C., 1999. Status of high-resolution satellite imaging, *Proceedings of Photogrammetric Week*' 99 (D. Fritsch and D. Hobbie, editors), Wichmann Verlag, Heidelberg, pp. 117–123.

Fraser, C.S., and H.B. Hanley, 2005. Bias-compensated RPCs for sensor orientation of high-resolution satellite imagery, *Photogrammetric Engineering & Remote Sensing*, 71(8):909–915.

Fritz, L.W., 1996. Commercial earth observation satellites, *International Archives of Photogrammetry and Remote Sensing, ISPRS Commission IV*, pp.273–282.

Habib, A., S.W. Shin, K. Kim, C. Kim, K. Bang, E.M. Kim, and D.C. Lee, 2007. Comprehensive analysis of sensor modeling alternatives for high-resolution imaging satellites, *Photogrammetric Engineering & Remote Sensing*, 73(11):1241–1251.

Hu, Y., and C.V. Tao, 2002. Updating solutions of the rational function model using additional control information, *Photogrammetric Engineering & Remote Sensing*, 68(7):715–723.

Jacobsen, K., 2007. Orientation of high resolution optical space images, *Proceedings of the 2007 Annual ASPRS Conference*, 07–11 May, Tampa, Florida, unpaginated CD-ROM.

Li, R., 1998. Potential of high-resolution satellite imagery for national mapping products, *Photogrammetric Engineering & Remote Sensing*, 64(12):1165–1170.

Li, R., G. Zhou, S. Yang, G. Tuell, N.J. Schmidt, and C. Fowler, 2000. A study of the potential attainable geometric accuracy of IKONOS satellite imagery, *Proceedings of the XIX$^{th}$ Congress of the International Society for Photogrammetry and Remote Sensing*, 16–23 July, Amsterdam, The Netherlands.

Li, R., K. Di, and R. Ma, 2003. 3-D shoreline extraction from IKONOS satellite imagery, *Marine Geodesy*, 26(1/2):107–115.

Li, R., F. Zhou, X. Niu, and K. Di, 2007. Integration of Ikonos and QuickBird imagery for geopositioning accuracy analysis, *Photogrammetric Engineering & Remote Sensing*, 73(9):1067–1074.

Li, R., X. Niu, C. Liu, B. Wu, and S. Deshpande, 2009. Impact of imaging geometry on 3D geopositioning accuracy of stereo Ikonos imagery, *Photogrammetric Engineering & Remote Sensing*, 75(9):1119–1125.

Mishra, D., S. Narumalani, D. Rundquist, and M. Lawson, 2006. Benthic habitat mapping in tropical marine environments using QuickBird multispectral data, *Photogrammetric Engineering & Remote Sensing*, 72(9):1037–1048.

Niu, X., K. Di, J. Wang, J. Lee, and R. Li, 2004. Geometric modeling and photogrammetric processing of high-resolution satellite imagery, *Proceedings of the XX$^{th}$ Congress of the International Society for Photogrammetry and Remote Sensing*, 12–23 July, Istanbul, Turkey, CD-ROM.

Qiao, G., W. Wang, and J. Zhang, 2007. 3D geo-positioning based on bias-compensated rational function model for QuickBird imagery, *Proceedings of SPIE, Geoinformatics 2007*, Nanjing, China, 25–26 May, pp.75212–75212.

QuickBird Imagery Products, 2008. *Product Guide*, DigitalGlobe, Inc,, Revision 4.7.4, September.

Tao, C.V., and Y. Hu, 2001. A comprehensive study of the rational function model for photogrammetric processing, *Photogrammetric Engineering & Remote Sensing*, 67(12): 1347–1357.

Tao, C.V., Y. Hu, and W. Jiang, 2004. Photogrammetric exploration of IKONOS imagery for mapping applications, *International Journal of Remote Sensing*, 25(14):2833–2853.

Toutin, T., 2004. DTM generation from Ikonos in-track stereo images using a 3D physical model, *Photogrammetric Engineering & Remote Sensing*, 70(6):695–702.

Toutin, T., 2006. Comparison of 3D physical and empirical models for generating DSMs from stereo HR images, *Photogrammetric Engineering & Remote Sensing,* 72(5):597–604.

Wang, J., K. Di, and R. Li, 2005. Evaluation and improvement of geopositioning accuracy of IKONOS stereo imagery, *ASCE Journal of Surveying Engineering*, 13(2):35–42.

Wanninger, L., 2003. Virtual reference stations (VRS), *GPS Solutions*, 7(2):143–144.

Warner, T.A., and K. Steinmaus, 2003. Spatial classification of orchards and vineyards with high spatial resolution panchromatic imagery, *Photogrammetric Engineering & Remote Sensing*, 71(2):179–187.

Xu, B., P. Gong, E. Seto, and R. Spear, 2003. Comparison of gray-level reduction and different texture spectrum encoding methods for land-use classification using a panchromatic Ikonos image, *Photogrammetric Engineering & Remote Sensing*, 69(5):529–536.

Zhou, G., and R. Li, 2000. Accuracy evaluation of ground points from Ikonos high-resolution satellite imagery, *Photogrammetric Engineering & Remote Sensing*, 66(9):1103–1112.

(Received 17 June 2009; accepted 21 September 2009; final version 02 December 2009)